PUBLICATION

MUSTANG

A MUltiple Space and Time scale Approach for the quaNtification of deep saline formations for CO_2 storaGe

Project Number:227286

AUTHORS: *Víctor Vilarrasa, Jesús Carrera, Diogo Bolster, Marco Dentz*

TITLE: *Semianalytical solution for CO_2 plume shape and pressure evolution during CO_2 injection in deep saline formations*

The research leading to these results has received funding from the European Community's Seventh Framework Programme [FP7/2007/2013) under grant agreement n° [227286]

Status	AUTHOR VERSION
Date	2013
Publisher	Springer
Reference	Transport in Porous Media, Vol. 97, pp 43-65

Peer reviewed paper

Title: Semianalytical solution for CO_2 plume shape and pressure evolution during CO_2 injection in deep saline formations

Authors: Víctor Vilarrasa, Jesús Carrera, Diogo Bolster and Marco Dentz

Journal published: Transport in Porous Media

Volume and pages: Vol. 97, pp. 43-65

Publication year: 2013

SEMIANALYTICAL SOLUTION FOR CO_2 PLUME SHAPE AND PRESSURE EVOLUTION DURING CO_2 INJECTION IN DEEP SALINE FORMATIONS

V. Vilarrasa[1,2], J. Carrera[1], D. Bolster[3] and M. Dentz[1]

[1] GHS, Institute of Environmental Assessment and Water Research (IDAEA), CSIC, Jordi Girona 18-26, 08034 Barcelona, Spain

[2] GHS, Dept Geotechnical Engineering and Geosciences, Technical University of Catalonia (UPC-BarcelonaTech), Jordi Girona 1-3, 08034 Barcelona, Spain

[3] Environmental Fluid Dynamics Laboratories, Department of Civil Engineering, University of Notre Dame, IN 46556, USA

ABSTRACT

The injection of supercritical carbon dioxide (CO_2) in deep saline aquifers leads to the formation of a CO_2 rich phase plume that tends to float over the resident brine. As pressure builds up, CO_2 density will increase because of its high compressibility. Current analytical solutions do not account for CO_2 compressibility and consider a volumetric injection rate that is uniformly distributed along the whole thickness of the aquifer, which is unrealistic. Furthermore, the slope of the CO_2 pressure with respect to the logarithm of distance obtained from these solutions differs from that of numerical solutions. We develop a semianalytical solution for the CO_2 plume geometry and fluid pressure evolution, accounting for CO_2 compressibility and buoyancy effects in the injection well, so CO_2 is not uniformly injected along the aquifer thickness. We formulate the problem in terms of a CO_2 potential that facilitates solution in horizontal layers, with which we discretize the aquifer. Capillary pressure is considered at the interface between the CO_2 rich phase and the aqueous phase. When a prescribed CO_2 mass flow rate is injected, CO_2 advances initially through the top portion of the aquifer. As CO_2 is being injected, the CO_2 plume advances not only laterally, but also vertically downwards. However, the CO_2 plume does not necessarily occupy the whole thickness of the aquifer. We found that even in the cases in which the CO_2 plume reaches the bottom of the aquifer, most of the injected CO_2 enters the aquifer through the layers at the top. Both CO_2 plume position and fluid pressure compare well with numerical simulations. This solution permits quick evaluations of the CO_2 plume position and fluid pressure distribution when injecting supercritical CO_2 in a deep saline aquifer.

NOMENCLATURE

b	thickness of the aquifer
b_c	thickness of the CO_2 plume at the injection well
d	thickness of a layer
g	Gravity
h_α	head of α-phase ($\alpha = c, w$)
J_α	mass flow rate per unit thickness of α-phase ($\alpha = c, w$)
k	intrinsic permeability
$k_{r\alpha}$	relative permeability of α-phase ($\alpha = c, w$)
n	number of layers
N_g	gravity number
P_0	reference fluid pressure corresponding to the hydrostatic pressure at depth z_0
P_{cc}	capillary entry pressure
P_α	fluid pressure of α-phase ($\alpha = c, w$)
Q_0	CO_2 volumetric flow rate
Q_m	prescribed CO_2 mass flow rate
Q_w	brine volumetric flow rate
$\mathbf{q}_\alpha$	volumetric flux of α-phase ($\alpha = c, w$)
R	radius of influence
r	radial coordinate
r_i	radial position of the interface at the depth z
r_{if}	interface position at the bottom of the CO_2 plume
r_p	radius of the injection well
S_α	degree of saturation of α-phase ($\alpha = c, w$)
S_{rw}	residual degree of saturation of brine
S_s	specific storage coefficient
t	Time
z	vertical coordinate
z_0	reference depth
Δz_j	thickness of layer j
z_f	depth of the bottom of the CO_2 plume
α	phase index, c for the CO_2 rich phase and w for the aqueous phase

β	CO_2 compressibility
ζ	vertical position of the CO_2 plume with respect to z_0
Φ_α	potential of α-phase ($\alpha = c, w$)
Φ_i	potential at the interface
Φ_R	potential at the radius of influence
φ	Porosity
μ_α	viscosity of α-phase ($\alpha = c, w$)
ρ_0	a reference CO_2 density corresponding to the reference pressure P_0
ρ_α	fluid density of α-phase ($\alpha = c, w$)

1. INTRODUCTION

Greenhouse gas emissions to the atmosphere can be reduced through the injection of supercritical carbon dioxide (CO_2) in deep saline aquifers. Under injection conditions, the density (450-900 kg/m^3) and viscosity (0.03-0.1 mPa·s) of CO_2 are highly dependent on pressure and temperature (Garcia, 2003). This density is sufficiently high for storage purposes, but it is much lower than that of typical resident waters (1020-1200 kg/m^3). Thus, the CO_2 plume tends to float above the resident brine and its thickness progressively increases as CO_2 pressure builds (Figure 1).

Existing analytical and most numerical solutions to this problem assume that the injection takes place uniformly along the whole thickness of the aquifer (Saripalli and McGrail, 2002; Nordbotten *et al*., 2005; Nordbotten and Celia, 2006; Dentz and Tartakovsky, 2009a; Vilarrasa *et al*., 2010a; Manceau and Rohmer, 2011; Houseworth, 2012). This assumption is unrealistic because of buoyancy. Instead, one should expect that CO_2 flows preferentially through the top portion of the aquifer, where the difference between CO_2 and resident water pressures are largest. In fact, the CO_2 plume may never

reach the bottom of the aquifer (Figure 1). Even analytical solutions that predict CO_2 plume evolution in the post-injection period consider that the CO_2 plume occupies the whole thickness of the aquifer at the end of the injection period (Hesse *et al*., 2007, 2008; Juanes *et al*., 2010). This may underestimate the CO_2 volume in free-phase at late times because the shape of the CO_2 plume at the end of injection affects its post-injection behaviour when capillary trapping is considered (MacMinn and Juanes, 2009).

Supercritical CO_2 is highly compressible relative to water and determining its density in the reservoir is complicated because of highly nonlinear and coupled relationships. On the one hand, CO_2 density depends on fluid pressure. On the other hand, fluid pressure buildup during injection depends on CO_2 density, because it determines the volume of displaced brine. Pressure buildup is also controlled by other factors, like caprock permeability (Birkholzer *et al*., 2009) or the nature of aquifer boundaries (Zhou *et al*., 2008). Resident brine can easily migrate out laterally in open aquifers. This limits pressure buildup, but may salinize adjacent freshwater bodies. By contrast, fluid and rock compressibility may limit storage capacity in the presence of low-permeability boundaries (Zhou *et al*., 2008; Mathias *et al*., 2011). Evidence that CO_2 density is difficult to estimate can be found both *in situ* (Nooner *et al*., 2007) and analytically (Vilarrasa *et al*., 2010a). While 3D seismic data gave an average *in situ* CO_2 density of 530 ± 65 kg/m^3 at the Utsira formation (Sleipner, Norway), the CO_2 density estimates prior to actual measurements ranged from 650 to 700 kg/m^3 (Nooner *et al*., 2007). CO_2 density, which is *a priori* unknown, has to be chosen when using an analytical solution to determine the CO_2 plume position. Neglecting CO_2 compressibility in these solutions can

lead to errors greater than 50 % in the CO_2 plume position at the top of the aquifer (Vilarrasa *et al*., 2010a).

In addition to the evolution of the CO_2 plume, it is important to understand the evolution of pressure. Pressure affects the required compression energy, the CO_2 density and the mechanical stability of the caprock (Rutqvist *et al*., 2007; Ferronato *et al*., 2010; Vilarrasa *et al*., 2012). Mathias *et al*. (2009) assumed the Nordbotten *et al*. (2005) solution for the CO_2 plume position to calculate a vertical average of the fluid pressure in the aquifer. The same result was obtained by Vilarrasa *et al*. (2010a), who extended the computation to the solution of Dentz and Tartakovsky (2009a) and to calculate fluid pressure at every point of the aquifer. However, the slope of CO_2 pressure as a function of the logarithm of distance obtained from these analytical solutions differs significantly from that of numerical solutions (Vilarrasa *et al*., 2010a).

This paper aims to develop a semianalytical solution to the CO_2 plume position and fluid pressure evolution accounting for CO_2 compressibility and buoyancy effects in the injection well, while acknowledging that CO_2 flux into the aquifer is not uniform along the aquifer thickness. Thus, the extent and the thickness of the CO_2 plume as well as the overpressure can be quickly assessed. We formulate the problem and present the methodology for solving it when the CO_2 mass flow rate or the CO_2 pressure are prescribed at the injection well. Finally, we present an application of this methodology and compare the results with full numerical simulations.

2. PROBLEM FORMULATION

Consider the injection of compressible CO_2 through a vertical well in a deep homogeneous horizontal confined brine aquifer. Mass conservation of these two fluids can be expressed as (Bear, 1972)

$$\frac{\partial(\rho_\alpha S_\alpha \varphi)}{\partial t} = -\nabla \cdot (\rho_\alpha \mathbf{q}_\alpha), \ \alpha = c, w, \tag{1}$$

where ρ_α is fluid density of the α-phase, S_α is the saturation of the α-phase, φ is porosity, t is time and $\mathbf{q}_\alpha$ is the volumetric flux of the α-phase, which can be either *c*, the CO_2 rich phase, or *w*, the aqueous phase.

Momentum conservation is expressed using Darcy's law

$$\mathbf{q}_\alpha = -\frac{k k_{r\alpha}}{\mu_\alpha}(\nabla P_\alpha + \rho_\alpha g \nabla z), \ \alpha = c, w, \tag{2}$$

where k is intrinsic permeability, $k_{r\alpha}$ is relative permeability of the α-phase, μ_α is viscosity of the α-phase, P_α is fluid pressure of α-phase, g is gravity and z is the vertical coordinate (positive upwards).

This two-phase flow is affected by buoyancy effects because CO_2 is lighter than brine. To quantify the relative influence of buoyancy we define a gravity number, N_g, as the ratio of gravity to viscous forces. Gravity forces can be represented by the buoyancy force ($\Delta\rho g$, where $\Delta\rho$ is the difference between fluids density) when Darcy's law is expressed in terms of equivalent head. Viscous dissipation forces correspond to the horizontal pressure gradient, which can be approximated as $(Q_0\mu/(2\pi r b k k_{r\alpha}))$, where Q_0 is the volumetric flow rate, r is radial distance and b is aquifer thickness). Still, since CO_2

is compressible, we prefer to express the volumetric flow rate in terms of the mass flow rate, Q_m, as $Q_0 = Q_m/\rho$. Thus, N_g becomes

$$N_g = \frac{2\pi r_{ch} b k k_{rc} \Delta\rho g \rho_{ch}}{\mu_c Q_m}, \tag{3}$$

where ρ_{ch} is a characteristic density and r_{ch} is a characteristic distance. Large values of the gravity number ($N_g >> 1$) indicate that buoyancy forces dominate. On the other hand, small gravity numbers ($N_g << 1$) indicate that viscous forces dominate. Note that buoyancy forces will always dominate far from the injection well, where r_{ch} is sufficiently large, whereas the opposite is generally true near the well, except for small mass flow rates and aquifers with a high permeability, in which case buoyancy forces will dominate also in the vicinity of the well.

Assuming that fluid density depends only on fluid pressure, the head of the α-phase is defined as (Bear, 1972)

$$h_\alpha = z - z_0 + \frac{1}{g}\int_{P_0}^{P_\alpha} \frac{\mathrm{d}P'_\alpha}{\rho_\alpha\left(P'_\alpha\right)}, \tag{4}$$

where h_α is the head of the α-phase, z_0 is a reference depth and P_0 is the hydrostatic fluid pressure corresponding to depth z_0.

Darcy's law can be expressed in terms of head provided that density is not affected by other variables (i.e. under isothermal conditions) by combining Eq. (2) and (4)

$$\mathbf{q}_\alpha = -\frac{k k_{r\alpha}}{\mu_\alpha}\rho_\alpha g \nabla h_\alpha . \tag{5}$$

When flow rate is prescribed at the injection well, CO_2 will penetrate initially along the top portion of the aquifer because its pressure is not sufficient to displace brine along

the entire aquifer thickness. As injection continues and CO_2 pressure builds up, the portion of the well occupied by CO_2 grows up to the depth where CO_2 pressure equilibrates with that of brine. As a result, the plume advances not only laterally, but also vertically downwards. Its thickness also increases with time (Figure 1). Brine and CO_2 pressures are related at the porous medium interface via the capillary entry pressure

$$P_c(r_i, z) = P_w(r_i, z) + P_{cc}, \tag{6}$$

where P_{cc} is the capillary entry pressure and r_i is the radial position of the interface at depth *z*.

Neglecting mass transfer across the interface, the problem is defined by the two differential equations in (1), one for each phase, which are coupled by the equilibrium equation in (6) and by the continuity of flux at the interface

$$\mathbf{q}_c(r_i, z) = \mathbf{q}_w(r_i, z). \tag{7}$$

The boundary condition at the injection well is applied at the top of the aquifer, where it is possible to prescribe either the total CO_2 mass flow rate or the CO_2 pressure. This formulation is realistic and leads naturally to non-uniform CO_2 flux into the aquifer along the well depth. As for the outer boundary, we consider an infinite aquifer.

3. SEMIANALYTICAL SOLUTION

3.1. *Radial injection of compressible CO_2*

To address the problem of CO_2 injection defined in the previous section we assume that the CO_2 rich phase and the formation brine are separated by a sharp interface. The validity of this assumption has been discussed extensively in previous studies on

analytical solutions (Nordbotten *et al*., 2005; Dentz and Tartakovsky, 2009a, 2009b; Lu *et al*., 2009). Capillary pressure is considered at the interface between the CO_2 rich phase and the formation brine (Eq. (6)). Thus, there is a jump in fluid pressure at the interface equal to the entry pressure. CO_2 dissolution into the brine, which may induce density-driven convective cells (Lindeberg and Wessel-Berg, 1997; Riaz *et al*., 2006; Hidalgo and Carrera, 2009; Pau *et al*., 2010), is not considered here.

We solve the problem by vertically discretizing the aquifer into *n* layers of equal thickness $d = b/n$ (Figure 2). The time evolution of the problem is solved using discrete time steps to overcome nonlinearities and coupling difficulties. The interface advances laterally in the layers that contain CO_2, but also moves vertically downwards as fluid pressure builds up. CO_2 at the bottom of the CO_2 plume may fill the thickness of a layer only partially. Once the CO_2 plume reaches a thickness equal to *md*, where *m* is the number of layers filled with CO_2, the following layer *m*+1, previously devoid of CO_2, begins to fill with CO_2. The part occupied by CO_2 in this new layer has a thickness equal to $b_c - md$, where b_c is the CO_2 plume thickness at the well (Figure 2).

To calculate the CO_2 plume thickness in the injection well, we assume hydrostatic conditions in it,

$$\frac{\mathrm{d}P_\alpha}{\mathrm{d}z} = -g\rho_\alpha\left(P_\alpha\right),\ \alpha = c, w\,. \tag{8}$$

This assumption is motivated by observations from high-resolution numerical simulations. Therefore, CO_2 enters the aquifer only through the part of the injection well occupied by CO_2; the mass flux will be higher at the top of the aquifer because of the larger difference between CO_2 and brine pressure.

To calculate the lateral advance of CO_2 in each layer, we assume that the hydraulic response within the CO_2 plume is much shorter than transport of the front. Therefore, we consider a quasi-steady (sequence of steady-states) description of the moving fronts in Eq. (1), i.e. the left-hand side of Eq. (1) cancels. Additionally, we make the Dupuit approximation of horizontal flow. Furthermore, the density of the CO_2 phase will vary in space due to changes in the CO_2 pressure and due to the high compressibility of CO_2. Therefore, conservation should not be expressed in terms of volumetric fluxes, but mass fluxes. The total mass flow rate, per unit aquifer thickness, in a radial injection varies with depth but is constant at a given *z* within each phase

$$J_\alpha = 2\pi r \rho_\alpha q_{r\alpha}, \tag{9}$$

where J_α is the mass flow rate per unit thickness of α-phase and $q_{r\alpha}$ is the horizontal component of the volumetric flux of α-phase. This mass flow rate per unit thickness will vary from layer to layer. At the interface in each layer, we impose continuity of flux in the radial direction

$$q_{rc}(r_j, z) = q_{rw}(r_j, z), \tag{10}$$

where r_j is the radius of the interface in layer j.

Since we adopt a sharp interface approximation, the saturation in the CO_2 rich phase is taken as constant. Thus, the interface position advances as

$$\frac{dr_j}{dt} = \frac{q_{r\alpha}(r_j)}{\varphi(1 - S_{rw})}, \tag{11}$$

where S_{rw} is the residual degree of saturation of brine.

To eliminate complexities associated with nonlinearity, we define the following potential to formulate the problem assuming that relative permeability and fluid density are solely a function of fluid pressure

$$\Phi_\alpha(h_\alpha) = \int_0^{h_\alpha} 2\pi g k k_{r\alpha}(h'_\alpha) \frac{\left(\rho^*_\alpha(h'_\alpha)\right)^2}{\mu_\alpha} \mathrm{d}h'_\alpha \,, \tag{12}$$

where $\rho^*_\alpha(h'_\alpha) = \rho^*_\alpha\left(P_\alpha(h'_\alpha)\right)$.

Combining Eq. (5), (9) and (12), flow rate in a layer becomes

$$r\frac{\mathrm{d}\Phi_\alpha}{\mathrm{d}r} = -J_\alpha \,. \tag{13}$$

Though we make the Dupuit approximation of horizontal flow within a layer, we acknowledge vertical CO_2 leakage between layers. Acknowledging that flow towards the top of the aquifer is largely buoyancy driven, we impose that the vertical mass flow rates between layers occur punctually, for simplicity. The distance at which the vertical flow rates are injected to the adjacent layer depends on the gravity number computed in the vicinity of the injection well (Eq. (3)). This is because vertical flow rates are expected to occur when gravity forces dominate, i.e. large gravity numbers. Then, vertical flow rates will occur close to the injection well for large gravity numbers. On the other hand, vertical flow rates will occur far from the injection well for small gravity numbers computed close to the injection well. Therefore, the distance at which the vertical flow rates occur is inversely proportional to the gravity number. The vertical mass flow rate of a layer to its adjacent one is given by

$$J_{cz,j} = \int_{r_p}^{r_j} 2\pi\rho_c q_{zc} \,\mathrm{d}r \,, \tag{14}$$

where r_p is the radius of the well and q_{zc} is the vertical component of the volumetric CO_2 flux. We will inject this flow rate at a radius $\bar{r}_j = \min\left(r_{j+1}, b/(2N_g)\right)$. The term $b/(2N_g)$ reflects the fact that the injection distance is inversely proportional to the gravity number as mentioned above. For simplicity, we have adopted r_{j+1} as $\bar{r}_j$. Introducing Eq. (5) into Eq. (14) and assuming that the CO_2 head varies linearly with the logarithm of distance to the well (we assume this based on previous experience and observations from high resolution numerical simulations, which will be presented in further detail in Section 5), after some algebra, yields

$$J_{cz,j} = \frac{2\pi k k_{rc} \rho_c^2 g}{\mu_c \Delta z_j} \left(u_j - u_{j+1}\right) \left(r_{j+1} - r_p - r_{j+1} \ln \frac{r_{j+1}}{r_p} \right), \tag{15}$$

where u_j is the logarithmic slope of the CO_2 head in layer j, Δz_j is the thickness of layer j and CO_2 density is evaluated at the point of the vertical flow rate injection. Note that the subscript of the layers increases with depth, i.e. layer j is placed above layer j+1.

The integration of Eq. (13), accounting for the fact that now J_c is a function of the radial distance due to the vertical flow rates, yields the solution of the problem

$$\Phi_{w,j} = \Phi_R + J_{w,j} \ln\left(\frac{R}{r}\right), \qquad r \geq r_j \tag{16a}$$

$$\Phi_{c,j} = \Phi_j + \left(J_{c,j} + J_{cz,j+1}\right) \ln\left(\frac{r_j}{r}\right), \qquad r_{j+1} < r < r_j \tag{16b}$$

$$\Phi_{c,j} = \Phi_j + J_{c,j} \ln\left(\frac{r_j}{r}\right) + J_{cz,j+1} \ln\left(\frac{r_j}{r_{j+1}}\right), \qquad r < r_{j+1} \tag{16c}$$

where Φ_R is the potential at the radius of influence, R is the radius of influence, the subscript after the comma indicates the layer (e.g. ,j indicates layer j) and Φ_j is the

potential at the interface in layer j . Φ_R is known and constant because it refers to the initial fluid pressure in the aquifer. Φ_j can be determined by evaluating Eq. (16a) at the interface. The radius of influence corresponds to the distance affected by the pressure buildup cone caused by injection and grows with the square root of time as

$$R = \sqrt{\frac{2.25k\rho_w gt}{\mu_w S_s}}, \tag{17}$$

where S_s is the specific storage coefficient. This result comes from combining the classical Theis and Thiem solution and is further discussed in Vilarrasa *et al*. (2010a).

The CO_2 mass flow rate at the injection well for layer *j* can be determined from Eq. (16c) as

$$J_{c,j} = \frac{\Phi_{c,j}(r_p) - \Phi_j - J_{cz,j+1}\ln(r_j/r_{j+1})}{\ln(r_j/r_p)}. \tag{18}$$

This CO_2 mass flow rate is different in every layer and will change with time as the CO_2 plume grows. The evolution of the CO_2 plume is calculated using a time stepping algorithm. Integrating Eq. (11) and using Eq. (9) yields the interface position for a given time step

$$r_j^{l+1}(z) = \sqrt{\left(r_j^l\right)^2 + \frac{J_{c,j}^l(r_j)\Delta t^{l+1}}{\pi\varphi(1-S_{rw})\rho_{ci,j}^l}}, \tag{19}$$

where superscript *l* denotes the time step, Δt is increment of time between step *l* and step *l*+1 and $\rho_{ci,j}$ is the CO_2 density at the interface in layer *j*.

The volumetric flow rate of brine, Q_w, at a radial distance *r* from the well can be calculated once the interface position is known. Due to the continuity of fluxes at the interface, we obtain

$$Q_w(r) = \int_{z_f}^{z_0-\zeta(r)} \frac{J_c(r)}{\rho_c(r)} \mathrm{d}z, \tag{20}$$

where z_f is the depth of the bottom of the CO_2 plume and ζ is the vertical position of the CO_2 plume from the top of the aquifer.

The volume of displaced brine at radius *r* is equal to the volume of injected CO_2. The flow rate of brine is driven by the overpressure produced by the injected CO_2, which is assumed to be distributed through the portion of the aquifer thickness occupied by the formation brine

$$Q_w(r) = -\int_{z_0-b}^{z_0-\zeta(r)} 2\pi r \frac{k}{\mu_w} \frac{\partial P_w}{\partial r} \mathrm{d}z. \tag{21}$$

Integrating Eq. (21) yields the following expression for brine pressure

$$P_w - P_0 = \frac{\mu_w Q_w(r)}{2\pi k(b-\zeta(r))} \ln\frac{R}{r}. \tag{22}$$

As mentioned above, two types of boundary conditions can be adopted at the injection well. Either a prescribed CO_2 mass flow rate or a prescribed CO_2 pressure can be imposed. In either case, the condition is imposed at the depth that coincides with the top of the aquifer. Both are discussed below.

3.2. *Prescribed CO_2 mass flow rate*

When injecting a prescribed CO_2 mass flow rate, the CO_2 plume advances both laterally and vertically downwards as CO_2 is injected. Since this problem presents two unknowns at every time step, i.e. the CO_2 head at the well and the thickness of the CO_2 plume at the well, two conditions are needed. First, hydrostatic conditions are assumed in the well (Eq. (8)). And second, mass balance must be satisfied. The mass inlet at a given

time step corresponds to the mass flow rate multiplied by the time increment. This mass is distributed through the layers containing CO_2 proportionally to the mass flow rate per unit thickness and the thickness of each layer. Furthermore, the mass that occupies the volume corresponding to the increment of the plume thickness in each time step has to be accounted for, resulting in

$$Q_m = \sum_{j=1}^{m} J_{c,j} \Delta z_j + \overline{\rho}_c \pi r_{if}^2 \varphi (1 - S_{rw}) \frac{\Delta z_f}{\Delta t}, \tag{23}$$

where Q_m is the prescribed CO_2 mass flow rate, m is the total number of layers in which CO_2 is present, $\overline{\rho}_c$ is the mean CO_2 density in the layer that coincides with the bottom of the CO_2 plume, r_{if} is the interface position at the bottom of the CO_2 plume and Δz_f is the increment of the CO_2 plume thickness at the well at a given time step.

3.3. *Prescribed CO_2 pressure*

Since the head at the well is known when imposing the CO_2 pressure, there is only one unknown: the thickness of the CO_2 plume at the well. Hence, imposing hydrostatic conditions in the well (Eq. (8)) and knowing that the bottom of the CO_2 plume in the well coincides with where the CO_2 pressure equals the brine pressure allows the problem to be solved.

4. ALGORITHM

The evolution of the position of the CO_2 plume is calculated using a time stepping algorithm. The process is very similar for the two possible injection boundary conditions

and is repeated for each time step (Figure 3). The procedure has to be initialized, using a small time increment, as follows

- The CO_2 plume is assumed to grow slightly in the top layer, i.e. the interface position advances laterally a fraction of the well radius and the thickness of the CO_2 plume is a fraction of *d*.
- The volumetric flow rate is assumed equal to the mass flow rate divided by density at the reference CO_2 pressure.

These two assumptions allow for initialization of the overpressure (using Eq. (22) and the volumetric flow rate), the potential at the interface (using Eq. (12)), the depth that the CO_2 plume reaches, the head at the injection well and the potential at the well (using Eq. (12)). No vertical flow rates exist in this initialization. After this, the time stepping algorithm can then be used. It is as follows

1. Determine the vertical CO_2 mass flow rate (Eq. (15)) and the horizontal CO_2 mass flow rate in each layer evaluating Eq. (18) at the well. We use the potential at the interface and at the well and the interface position evaluated at the previous time step.
2. Calculate the new interface position in every layer using Eq. (19). The CO_2 mass flow rate is the one calculated in step 1 and the CO_2 density at the interface is the one evaluated at the previous time step.
3. Calculate the potential at the interface (Eq. (12)), using Eq. (20) to calculate the volumetric flow rate and Eq. (22) to calculate the brine pressure, and Eq. (6) to calculate the CO_2 pressure at the interface.

4.1. Impose a prescribed CO_2 mass flow rate: solve the system of two equations (Eqs. (23) and (8)) and determine the CO_2 head at the well and the thickness of the CO_2 plume at the well.

4.2. Impose a prescribed CO_2 pressure: the head at the well can be determined by using Eq. (4) and the thickness of the CO_2 plume at the well can be calculated by imposing Eq. (8).

5. Based on the head at the well calculated in step 4, compute the potential at the well using Eq. (12).

These five steps are repeated, applying a time increment after every loop, until the desired time of CO_2 injection is completed. The time increment should be small (some seconds) at the beginning of injection and can progressively increase (up to some hours). We found a condition that the thickness by which the CO_2 plume increases should be less than a small percentage of the thickness of a layer (typically less than a 3 %) in order to guarantee convergence.

5. APPLICATION

5.1. *Spreadsheet programming*

In order to evaluate this methodology, we programmed it in a spreadsheet that can be downloaded from GHS (2012). We programmed it this way to highlight the ease of implementation and use by non-expert programmers. This implementation considers 25 layers. We chose 25 layers, because we found this sufficient to resolve all features and that the result barely changed as this number increases. In fact the solution already

changes very little from 10 to 25 layers as illustrated in Figure 3. Note that the solutions presented in Figure 3 do not incorporate vertical flows. The implementation requires a prescribed mass flow rate, constant properties of the brine (density and viscosity), constant CO_2 viscosity and the CO_2 density is defined to vary linearly with CO_2 pressure

$$\rho_c = \rho_0 + \beta\left(P_c - P_0\right), \tag{24}$$

where ρ_0 is the reference density for the reference pressure P_0 and β is CO_2 compressibility. For the range of pressures in this study this linear approximation appears to provide good results. The parameter values in (24) are taken from the data tables given by Span and Wagner (1996).

With this linear approximation of the CO_2 density, the potential for the CO_2 can be obtained by integrating Eq. (12), which yields (see Appendix A)

$$\Phi_c = \frac{\pi k \rho_0^2}{\mu_c \beta} e^{-2g\beta(z-z_0)}\left(e^{2g\beta h_c} - 1\right). \tag{25}$$

Furthermore, CO_2 pressure can be expressed as a function of the potential (Appendix A)

$$P_c - P_0 = \sqrt{\frac{\mu_c}{\pi k \beta}\Phi_c + \frac{\rho_0^2}{\beta^2} e^{-2g\beta(z-z_0)}} - \frac{\rho_0}{\beta}. \tag{26}$$

Note that CO_2 overpressure varies with the square root of the logarithm of the distance to the injection well (see the form of the potential Φ_c in Eq. (16b,c)).

The solution of the system of two equations (Eqs. (8) and (23)) for finding the CO_2 head and the thickness of the CO_2 plume at the well is shown in Appendix B. CO_2 pressure is calculated by solving the system of two equations with two unknowns presented in Appendix B and brine pressure is given by the overpressure that CO_2

generates when brine is displaced. The mean density appearing in Eq. (23) is calculated in Appendix C.

5.2. *Model setup*

We represent a 100 m thick saline aquifer whose top is located at a depth of 1000 m. The aquifer is assumed to be infinite-acting, homogeneous and isotropic. The permeability of the aquifer is either 10^{-12} or 10^{-13} m^2, its porosity is 0.1 and the rock compressibility is $1.2 \cdot 10^{-10}$ Pa^{-1}. The temperature is assumed to be constant and equal to 320 K. The density of brine is 1087.5 kg/m^3, its viscosity is 0.6 mPa·s and its compressibility is $4.5 \cdot 10^{-10}$ Pa^{-1}. Thus, the specific storage coefficient yields a value of $1.76 \cdot 10^{-6}$ m^{-1}. The reference CO_2 density ρ_0, corresponding to the reference pressure $P_0 = 10$ MPa (hydrostatic pressure at the top of the aquifer), is 448.28 kg/m^3 and its compressibility β is $5.56 \cdot 10^{-5}$ $kg/m^3 \cdot Pa^{-1}$ (Span and Wagner, 1996). β is the product of the actual CO_2 compressibility and a density. The actual CO_2 compressibility at the pressure and temperature of the aquifer is $1.48 \cdot 10^{-7}$ Pa^{-1}. Note that CO_2 compressibility, for the range of pressure and temperature of this study, is three orders of magnitude higher than that of brine. The CO_2 viscosity is calculated using the expression proposed by Altunin and Sakhabetdinov (1972). Though constant, CO_2 viscosity is case specific and depends on the overpressure and aquifer temperature, so that a representative value can be adopted according to the mean CO_2 density. CO_2 viscosity is set, according to pressure and temperature, to 0.03 and 0.04 mPa·s for the aquifer with a permeability of 10^{-12} and 10^{-13} m^2, respectively. The entry pressure equals 0.02 MPa and the residual degree of saturation of brine is 0.025. The injected mass flow rate is 1.0 Mt/yr. An

injection ramp is used to progressively increase the mass flow rate from zero to the desired mass flow rate. Doing so, the increments in the CO_2 plume thickness are small. This injection ramp lasts less than 50 s, so its effect can be considered as negligible over the course of the full injection period for practical purposes.

The finite element numerical code CODE_BRIGHT (Olivella *et al.*, 1994; 1996), extended for CO_2 sequestration (Vilarrasa *et al.*, 2010b), has been used to validate the results of this semianalytical solution with those of numerical results. The aquifer is represented by an axisymmetric model, with a radius of 100 km, in which CO_2 is injected at the top of the injection well. The radius of the injection well is 0.5 m. The well is represented by a zone of unit porosity and high permeability (four orders of magnitude higher than that of the aquifer). The inclusion of the injection well in the model allows us to reproduce a realistic CO_2 injection, with non-uniform CO_2 flux along the whole thickness of the aquifer. The grid is structured and has 25 elements in the vertical coordinate, which matches the 25 layers adopted in the application of the semianalytical solution. We used a van Genuchten retention curve (van Genuchten, 1980), with an entry pressure of 0.02 MPa and a shape parameter of 0.8. The relative permeability functions, for both the CO_2 and the brine, are linear with the degree of saturation of each phase. These retention curve and relative permeability functions produce a CO_2 plume with an almost constant CO_2 saturation and a narrow capillary fringe. Thus, the numerical solutions are close to the assumption of the abrupt interface approximation assumed for the semianalytical solution. The CO_2 saturation 90 % isoline has been chosen to represent the position of the CO_2-brine interface. The effect of changing the retention curve would be a wider capillary fringe and a non constant CO_2 saturation within the CO_2 plume.

However, the shape of the plume would be maintained. Thus, the geometry of the CO_2 plume can be calculated precisely by introducing into the semianalytical solution an appropriate value of the residual degree of saturation of brine. CO_2 pressure would change slightly due to capillarity, but its profile with respect to the logarithm of distance would be maintained. However, the curvature of the relative permeability curves affects the thickness of the CO_2 plume tip at the top of the aquifer (Gasda *et al*., 2008). A more concave relative permeability curve, such as the cube of the degree of saturation of each phase compared to a linear relationship with the degree of saturation, yields a wider CO_2 plume tip.

5.3. *Validation of the semianalytical solution*

We compare the results of the semianalytical solution with those of the numerical solution. Additionally, the analytical solutions of Nordbotten *et al*. (2005) and Dentz and Tartakovsky (2009a), in which the method proposed by Vilarrasa *et al*. (2010a) to incorporate CO_2 compressibility have been applied, are presented for comparative purposes. As mentioned earlier, these analytical solutions inject CO_2 uniformly along the whole thickness of the aquifer. Figure 5 displays the mass flow rate per unit thickness as a function of depth in the injection well, showing that most of the CO_2 enters into the aquifer through its top portion, rather than uniformly along the whole thickness of the aquifer. Whereas this may not be desirable from a storage point of view, where it is desirable to maximize the use of pore space, it will occur whenever the flow rate is small for the aquifer permeability.

Figure 6 displays the CO_2 plume position for the analytical, semianalytical and numerical solutions after 1 yr of injecting 1 Mt/yr of CO_2 for two aquifer permeabilities. We consider a case with high permeability ($k = 10^{-12}$ m^2) in which gravity forces dominate and another case with low permeability ($k = 10^{-13}$ m^2) in which viscous forces dominate. The semianalytical solution compares well with the numerical solution in both cases. The CO_2 plume occupies only the top portion of the aquifer when gravity forces dominate (CO_2 is injected into the aquifer through the top 32 m) (Figure 6a). On the other hand, the CO_2 plume reaches the bottom of the aquifer when viscous forces dominate (Figure 6b). The Nordbotten *et al*. (2005) solution gives a better approximation when viscous forces dominate, while the Dentz and Tartakovsky (2009a) solution predicts a better CO_2 plume position when gravity forces dominate. However, both analytical solutions differ from the numerical solution at the bottom of the CO_2 plume due to the fact that they consider a uniform injection along the whole thickness of the aquifer.

Figure 7 compares fluid overpressure at the top of the aquifer as a function of the distance to the injection well resulting from the semianalytical, numerical and analytical solutions when injecting 1.0 Mt/yr in an aquifer with a permeability of 10^{-13} m^2. Fluid overpressure obtained from the semianalytical solution compares well with that of the numerical solution, presenting the same slope in the region occupied by CO_2 close to the injection well. The pressure drop increases sharply at the distance where CO_2 from the second layer is injected in the top layer. This is in contrast with the numerical solution, where the gradient increases smoothly. As a result, our solution is somewhat more abrupt than the numerical solution near the interface. Existing analytical solutions, i.e. those of Nordbotten *et al*. (2005) and Dentz and Tartakovsky (2009a), fail to give good fluid

pressure predictions. First, they predict a lower brine overpressure because they underestimate the volumetric flow rate of brine. This is because CO_2 is injected along the whole thickness of the aquifer and since CO_2 density increases with depth, the mean CO_2 density becomes higher than in the semianalytical and numerical solutions. Additionally, the slopes of fluid pressure inside the CO_2 plume are lower than that of numerical simulations. In contrast, the slope of the semianalytical solution is the same as that of the numerical solution close to the injection well in the region occupied by CO_2. Hence, it can be concluded from this semianalytical solution that while brine overpressure is proportional to the logarithm of distance from the injection well, CO_2 overpressure is proportional to the square root of the logarithm of the distance from the injection well (recall Eq. (26)).

Figure 8 displays the evolution of the overpressure at the injection well when injecting 1.0 Mt/yr in an aquifer with a permeability of 10^{-13} m^2. While the overpressure predicted by the analytical solutions of Nordbotten *et al*. (2005) and Dentz and Tartakovsky (2009a) increases continuously, fluid overpressure decreases after reaching a maximum at the beginning of injection for the semianalytical and numerical solutions. Mukhopadhyay *et al*. (2012) found that overpressure increases continuously when injecting CO_2 in depleted gas reservoirs, whose fluid pressure is significantly below hydrostatic conditions. However, a pressure drop after the initial pressure buildup was observed *in situ* in the Ketsin test site, Germany (Henninges *et al*., 2011) and numerically by Vilarrasa *et al*. (2010b), who argued that pressure drops because the overpressure that occurs in the capillary fringe due to relative permeability reduction is distributed over a

larger area as the CO_2 plume increases and because the viscosity of the CO_2 is much lower than that of the brine.

5.4. *CO_2 plume thickness*

Figure 9 shows the CO_2 plume position evolution for several injection times given by the semianalytical solution when injecting 1.0 Mt/yr in an aquifer with a permeability of 10^{-13} m^2. CO_2 advances laterally and vertically downwards with injection time. Note that the CO_2 plume advances preferentially through the top of the aquifer for increasing injection times. This is because gravity forces become dominant as CO_2 flows away from the injection well. Note that in this case the CO_2 plume reaches the aquifer bottom for an injection time longer than 30 days (actually, it occurs after 162.6 days of injection). However, the CO_2 plume would not reach the bottom of the aquifer in a more permeable aquifer, like the one presented in Figure 6a.

Figure 10 displays the CO_2 plume thickness at the well after 1 yr of injection as a function of the gravity number computed at 1 m from the injection well (Eq (3)) for several aquifer permeabilities. The curves are obtained by varying the mass flow rate. The logarithm of the CO_2 plume thickness decreases linearly with the logarithm of the gravity number, presenting a slope of -1/2. The CO_2 plume is thinner than the aquifer thickness for high gravity numbers (buoyancy forces dominate). In contrast, it reaches the bottom of the aquifer for gravity numbers lower than 0.15 (viscous forces dominate). The effect of permeability is small, but not negligible because permeability affects fluid overpressure and thus CO_2 density. These curves are useful for quickly estimating the CO_2 thickness at the well of a CO_2 injection project.

6. DISCUSSION AND CONCLUSIONS

We have presented a semianalytical solution for the CO_2 plume geometry and fluid pressure evolution that accounts for CO_2 compressibility and buoyancy in the well. The latter enables us to study the non-uniform injection rate along the aquifer thickness that will occur in industrial injection sites (Figure 5). CO_2 compressibility is taken into account by assuming that CO_2 density varies linearly with CO_2 pressure. This approximation is reasonable because CO_2 pressure is relatively constant during injection (recall Figure 8). However, if the range of variation were wider, an exponential approximation would adjust better to the actual CO_2 density variation with pressure. To achieve a non-uniform injection along the aquifer thickness, we assume that fluid pressure is hydrostatic within the well, though its magnitude changes with time. This reflects the low viscosity of CO_2 and the slow velocities that will occur in real sites. Indeed, fluid pressure is observed to be hydrostatic inside the well in the numerical simulations of the detailed problem. While the general methodology presented allows for variable viscosity the specific implementation in this work assumes constant viscosity for simplicity. However, since it is an input parameter, it can be adjusted according to the aquifer temperature and the overpressure induced by injection in each case. This implementation has 25 horizontal layers, which provides a reasonable resolution in many cases, except for very thick aquifers (of 250-300 m thick or thicker), where more layers may be necessary.

We found that both CO_2 plume position and fluid pressure obtained from the proposed semianalytical solution compare well with those given by numerical

simulations. Analytical solutions, which have been corrected to account for CO_2 compressibility to make them comparable with the semianalytical and numerical solutions, give acceptable results of the CO_2 plume position depending on the gravity number (Figure 6). However, the semianalytical solution gives good estimates regardless of the gravity number. Nonetheless, a weakness of the semianalytical solution is that vertical flows have to be considered explicitly between adjacent layers, otherwise the CO_2 plume shape does not resemble that of numerical simulations (compare Figures 4 and 6). Another limitation is that the semianalytical solution yields good estimates of the CO_2 plume tip only for a relative permeability curve that is linear with the degree of saturation of each phase. For more concave relative permeability curves (e.g. the cube of the degree of saturation of each phase), the CO_2 plume tip becomes thicker and cannot be precisely reproduced by the semianalytical solution. Nevertheless, the approximation of the semianalytical solution has a clear advantage over numerical solutions in terms of the time required for calculation. One should bear in mind that simulating CO_2 injection through the well instead of injecting it uniformly along the whole thickness of the aquifer results in high computational cost. By contrast, the semianalytical solution gives immediate results. Furthermore, analytical and semianalytical solutions can be coupled with numerical models in order to speed up their calculations (Celia and Nordbotten, 2009; McDermott *et al*., 2011).

This solution facilitates quick evaluation of the lateral extension and thickness of the CO_2 plume, which may not reach the bottom of the aquifer, for a given injection time. The calculation of the CO_2 plume thickness accounting for buoyancy is innovative and significant because it points out important differences to calculations that are based on

the commonly accepted assumption that the CO_2 plume occupies the whole aquifer thickness. The CO_2 plume thickness is a function of the gravity number (see Figure 10). This knowledge can be useful to support decision-making concerning the operation of CO_2 injection projects. Additionally, this solution can be helpful in designing and interpreting CO_2 injection tests in pilot projects. In this context, it is important to bear in mind that, from a storage point of view, it is desirable to inject over the whole aquifer thickness to maximize the use of pore space. As we have seen, this goal is limited by buoyancy, which dominates far from the injection well. However, even near the well, injecting over a partial thickness may be profitable during early stages because it promotes CO_2 dissolution into the brine, which in turn may cause mineral dissolution and stimulation (i.e. increasing the permeability of the aquifer, so that injectivity increases and the required overpressure to inject a given mass flow rate decreases, which reduces injection costs). This stimulation close to the well can propagate relatively far from the injection well by promoting CO_2 advance through the top of the aquifer. For such goal, our solution, generalized for varying permeability, would be extremely useful.

Finally, the slope of CO_2 pressure as a function of the logarithm of distance from the well calculated with the semianalytical solution is the same as that of the numerical solution. In the semianalytical solution, the CO_2 overpressure varies with the square root of the logarithm of the distance to the injection well (Eq. (26)). This is interesting because this variation with distance to the well differs from those of existing analytical solutions. Additionally, the semianalytical solution reproduces a CO_2 injection pressure evolution similar to the one observed in numerical solutions and in field-scale injection projects, i.e. fluid pressure drops after an initial abrupt fluid pressure buildup. This

behaviour, which appears naturally in this semianalytical solution, is not reflected by other existing analytical solutions.

APPENDIX A

Here we develop the mathematical formulation of the problem for the case in which CO_2 density varies linearly with pressure (Eq. (24)), and CO_2 viscosity and brine properties are constant.

First, we integrate Eq. (4) for the CO_2 phase, which yields

$$h_c = z - z_0 + \frac{1}{g\beta}\ln\left(1+\frac{\beta}{\rho_0}\left(P_c - P_0\right)\right). \tag{A1}$$

The inverse of Eq. (A1) gives the CO_2 pressure as a function of the head as

$$P_c - P_0 = \frac{\rho_0}{\beta}\left(e^{g\beta(h_c-(z-z_0))}-1\right). \tag{A2}$$

Integrating Eq. (12) and using Eq. (A2) gives the following expression for the CO_2 potential

$$\Phi_c = \frac{\pi k \rho_0^2}{\mu_c \beta} e^{-2g\beta(z-z_0)}\left(e^{2g\beta h_c}-1\right). \tag{A3}$$

Since the exponent $2g\beta h_c$ is small, $\left(e^{2g\beta h_c}-1\right)$ can be approximated as $2g\beta h_c$. Therefore, the CO_2 potential can be expressed as

$$\Phi_c \approx 2\pi g k \frac{\rho_0^2}{\mu_c} h_c\, e^{-2g\beta(z-z_0)}, \tag{A4}$$

where the potential is composed of a part corresponding to a constant CO_2 density (ρ_0) multiplied by a correction due to CO_2 compressibility (the exponential in the right-hand

side of Eq. (A4)). Combining Eq. (A1) and (A3) and operating, yields an expression of CO_2 pressure as a function of the potential

$$P_c - P_0 = \sqrt{\frac{\mu_c}{\pi k \beta}\Phi_c + \frac{\rho_0^2}{\beta^2}e^{-2g\beta(z-z_0)}} - \frac{\rho_0}{\beta}. \tag{A5}$$

Note that the head (Eq. (A1)) at the interface can be expressed as a function of the CO_2 density as

$$h_{ci} = z - z_0 + \frac{1}{g\beta}\ln\left(\frac{\rho_0 + \beta\left(P_{ci} - P_0\right)}{\rho_0}\right) = z - z_0 + \frac{1}{g\beta}\ln\left(\frac{\rho_{ci}}{\rho_0}\right), \tag{A6}$$

where the subscript *i* indicates interface. Combining Eq. (A3) with Eq. (A6) yields the following expression for the CO_2 potential at the interface

$$\Phi_i = \frac{\pi k \rho_0^2}{\mu_c \beta}\left(\frac{\rho_{ci}^2}{\rho_0^2} - e^{-2g\beta(z-z_0)}\right). \tag{A7}$$

In the brine phase, integration of Eq. (4) yields

$$h_w = z - z_0 + \frac{P_w - P_0}{\rho_w g} \tag{A8}$$

which is the expression of the head for an incompressible fluid. Integrating Eq. (12) gives the potential in the brine phase as

$$\Phi_w = 2\pi g k \frac{\rho_w^2}{\mu_w} h_w. \tag{A9}$$

Combining Eq. (A8) with (A9), gives the following expression for the brine pressure

$$P_w - P_0 = \frac{\mu_w}{2\pi k \rho_w}\Phi_w - \left(z - z_0\right)\rho_w g. \tag{A10}$$

Note that the brine pressure varies with the logarithm of the distance to the injection well (see the form of the potential in Eq. (16a)).

APPENDIX B

A system of two equations with two unknowns has to be solved in step 4 of the time stepping algorithm when a mass flow rate is prescribed at the injection well. The unknowns are the head at the well and the thickness of the CO_2 plume at the well. The two equations are Eq. (23) and (8).

Combining Eq. (23) with Eqs. (18), (A3) and (A7), after some algebra, gives the following expression for the head at the well as a function of the increment of the CO_2 plume thickness

$$e^{2g\beta h_c} = \frac{Q - A_1 \Delta z_f + A_2 - A_3}{A_4}, \tag{B1}$$

where

$$Q = \frac{\mu_c \beta}{\pi k \rho_0^2} Q_m, \tag{B2a}$$

$$A_1 = \frac{\mu_c \beta}{\pi k \rho_0^2} \frac{\bar{\rho}_c \pi r_{if}^2 \varphi (1 - S_{rw})}{\Delta t}, \tag{B2b}$$

$$A_2 = \sum_{j=1}^{m} \frac{\rho_{ci,j}^2 / \rho_0^2}{\ln(r_j / r_p)} \Delta z_j, \tag{B2c}$$

$$A_3 = \frac{\mu_c \beta}{\pi k \rho_0^2} \sum_{j=1}^{n} \frac{J_{cz,j+1} \ln(r_{j+1} / r_j)}{\ln(r_j / r_p)} \Delta z_j, \tag{B2d}$$

$$A_4 = \sum_{j=1}^{m} \frac{e^{-2g\beta(z_j - z_0)}}{\ln(r_j / r_p)} \Delta z_j. \tag{B2e}$$

Next, assuming hydrostatic conditions at the well (Eq. (8)) and that the bottom of the CO_2 plume coincides where brine pressure equals CO_2 pressure and using Eqs. (A3) and (A5) give the second equation of the system of equations

$$e^{g\beta h_c} = p + \frac{\rho_w}{\rho_0} g\beta \Delta z_f \,, \tag{B3}$$

where

$$p = \frac{\beta}{\rho_0} P_w\left(z_{f-1}\right) + 1, \tag{B4}$$

where $P_w\left(z_{f-1}\right)$ is the brine pressure evaluated at the depth reached by the CO_2 plume in the previous time step. The combination of Eq. (B1) and (B3) gives the following quadratic equation

$$\Delta z_f^2 + B\Delta z_f + C = 0\,, \tag{B5}$$

where

$$B = \frac{2p\rho_0}{g\beta\rho_w} + \frac{\rho_0^2 e^{-2g\beta\left(z_f - z_0\right)}}{\rho_w^2 g^2 \beta^2} \frac{A_1}{A_4}\,, \tag{B6a}$$

$$C = \frac{\rho_0^2}{\rho_w^2 g^2 \beta^2}\left(p^2 - \frac{Q + A_2 - A_3}{A_4} e^{-2g\beta\left(z_f - z_0\right)} \right). \tag{B6b}$$

Once Eq. (B5) is solved and the increment of the CO_2 plume thickness at the well in a given time step is known, the head at the well can be calculated from Eq. (B1) as

$$h_c\left(r_p\right) = \frac{1}{2g\beta} \exp\left(\frac{Q - A_1 \Delta z_f + A_2 - A_3}{A_4} \right). \tag{B7}$$

APPENDIX C

The mean CO_2 density in a given layer has to be calculated in order to apply Eq. (23). Assuming that CO_2 density varies linearly with pressure (Eq. (24)), and using Eq. (A5),

(16c) and (A7), after some algebra, the following expression for the CO_2 density is obtained

$$\rho_c = \sqrt{\rho_{ci}^2 + \frac{\mu_c \beta}{\pi k} J_c \ln \frac{r_j}{r}} \ . \tag{C1}$$

The mean CO_2 density in a layer is obtained from dividing the CO_2 mass in a given layer by the volume that it occupies

$$\overline{\rho} = \frac{1}{V} \int_{z_{j-1}}^{z_j} \int_{r_p}^{r_j} 2\pi r \varphi (1 - S_{rw}) \rho_c \, \mathrm{d}r \, \mathrm{d}z \ . \tag{C2}$$

Introducing Eq. (C1) in Eq. (C2) and integrating yields

$$\begin{aligned} \overline{\rho} = & \frac{1}{\left(r_j^2 - r_p^2\right)} \left[r^2 \sqrt{a - b \ln r} - \frac{1}{2} \sqrt{\frac{\pi}{2}} \sqrt{b} e^{2a/b} erf\left(\sqrt{\frac{2}{b}} \sqrt{a - b \ln r} \right) \right]_{r_p}^{r_j} = \\ & \frac{1}{\left(r_j^2 - r_p^2\right)} \left[r_j^2 \rho_{ci} - r_p^2 \rho_{cp} + \frac{r_j^2}{2} \sqrt{\frac{b\pi}{2}} \exp\left(\frac{2\rho_{ci}^2}{b} \right) \left(erf\left(\sqrt{\frac{2}{b}} \rho_{ci} \right) - erf\left(\sqrt{\frac{2}{b}} \rho_{cp} \right) \right) \right] \end{aligned} , \tag{C3}$$

where

$$a = \rho_{ci}^2 + \frac{\mu_c \beta}{\pi k} J_c \ln r_j \, , \tag{C4a}$$

$$b = \frac{\mu_c \beta}{\pi k} J_c \, . \tag{C4b}$$

ACKNOWLEDGEMETS

V.V. wishes to acknowledge the Spanish Ministry of Science and Innovation (MCI), through the “Formación de Profesorado Universitario”, and the “Colegio de Ingenieros de Caminos, Canales y Puertos – Catalunya” for their financial support. This work has been funded by Fundación Ciudad de la Energía (Spanish Government) (www.ciuden.es) and

by the European Union through the “European Energy Programme for Recovery” and the Compostilla OXYCFB300 project. We also want to acknowledge the financial support received from the ‘MUSTANG’ (www.co2mustang.eu) and ‘PANACEA’ (www.panacea-co2.org) projects (from the European Community’s Seventh Framework Programme FP7/2007-2013 under grant agreements nº 227286 and nº 282900, respectively).

REFERENCES

Altunin, VV and Sakhabetdinov, MA (1972). Viscosity of liquid and gaseous carbon dioxide at temperatures 220-1300 K and pressure up to 1200 bar. *Teploenergetika*, 8:85-89.

Bear, J (1972). Dynamics of fluids in porous media. Elsevier, New York.

Birkholzer, JT, Zhou, Q and Tsang, C-F (2009). Large-scale impact of CO_2 storage in deep saline aquifers: A sensitivity study on pressure response in stratified systems. *International Journal of Greenhouse Gas Control*, 3:181–94.

Celia, MA and Nordbotten, JM (2009). Practical modeling approaches for geological storage of carbon dioxide. *Ground Water* 47 (5):627–638.

Dentz, M and Tartakovsky, DM (2009a). Abrupt-interface solution for carbon dioxide injection into porous media. *Transport In Porous Media* 79:15–27.

Dentz, M. and Tartakovsky, D.M. (2009b). Response to “Comments on abrupt-interface solution for carbon dioxide injection into porous media by Dentz and Tartakovsky (2008)" by Lu *et al*. *Transport In Porous Media* 79:39–41.

Ferronato, M, Gambolati, G, Janna, C and Teatini, P (2010). Geomechanical issues of anthropogenic CO_2 sequestration in exploited gas fields. *Energy Conversion & Management*, 51:1918–1928.

Garcia, JE (2003). Fluid Dynamics of Carbon Dioxide Disposal into Saline Aquifers. PhD thesis, University of California, Berkeley.

Gasda, SE, Celia, MA and Nordbotten, JM (2008). Upslope plume migration and implications for geological CO_2 sequestration in deep saline aquifers. *The IES Journal Part A: Civil & Structural Engineering*, 1:2-16.

GHS (Hydrogeology Group) (2012). Spreadsheet with the semianalytical solution for CO_2 injection. http://www.h2ogeo.upc.es/publicaciones/2011/Semianalytical_solution.xlsx

Henninges, J, Liebscher, A, Bannach, A, Brandt, W, Hurter, S, Köhler, S, Möller, F and CO_2SINK Group (2011). P-T-ρ and two-phase fluid conditions with inverted density profile in observation wells at the CO_2 storage site at Ketsin (Germany). *Energy Procedia*, 4:6085-6090.

Hesse, MA, Tchelepi, HA, Cantwell, BJ and Orr, FM Jr (2007). Gravity currents in horizontal porous layers: transition from early to late self-similarity, *Journal of Fluid Mechanics*, 577:363-383.

Hesse, MA, Tchelepi, HA and Orr, FM Jr (2008). Gravity currents with residual trapping. *Journal of Fluid Mechanics*, 611:35-60.

Hidalgo, JJ and Carrera, J (2009). Effect of dispersion on the onset of convection during CO_2 sequestration. *Journal of Fluid Mechanics*, 640:441-452.

Houseworth, JE (2012). Matched boundary extrapolation solutions for CO_2 well-injection into a saline aquifer. *Transport In Porous Media* 91:813–831.

Juanes, R, MacMinn, CW and Szulczewski, ML (2010). The footprint of the CO_2 plume during carbon dioxide storage in saline aquifers: storage efficiency for capillary trapping at the basin scale. *Transport In Porous Media*, 82**(**1):19-30, doi:10.1007/s11242-009-9420-3.

Lindeberg, E and Wessel-Berg, D (1997). Vertical convection in an aquifer column under a gas cap of CO_2. *Energy Conversion & Management*, 38:S229–S234.

Lu, C, Lee, S-Y, Han, WS, McPherson, BJ and Lichtner, PC (2009). Comments on "Abrupt-interface solution for carbon dioxide injection into porous media" by M. Dentz and D. M. Tartakovsky. *Transport In Porous Media* 79:29–37.

MacMinn, CW and Juanes, R (2009). Post-injection spreading and trapping of CO_2 in saline aquifers: impact of the plume shape at the end of injection. *Compututational Geoscience* 13:483-491.

Manceau, J-C and Rohmer, J (2011). Analytical solution incorporating history-dependent processes for quick assessment of capillary trapping during CO_2 geological storage. *Transport In Porous Media* 90:721–740.

Mathias, SA, Hardisty, PE, Trudell, MR and Zimmerman, RW (2009). Approximate solutions for pressure buildup during CO_2 injection in brine aquifers. *Transport In Porous Media*, 79(2):265-284.

Mathias, SA, González Martínez de Miguel, GJ, Thatcher, KE and Zimmerman, RW (2011). Pressure buildup during CO_2 injection into a closed brine aquifer. *Transport In Porous Media*, 89 (3):383-397.

McDermott, CI, Bond, AE, Wang, W and Kolditz, O (2011). Front tracking using a hybrid analytical finite element approach for two-phase flow applied to supercritical CO_2 replacing brine in a heterogeneous reservoir and caprock. *Transport In Porous Media* 90:545–573.

Mukhopadhyay, S, Yang, S-Y and Yeh, H-D (2012). Pressure buildup during supercritical carbon dioxide injection from a partially penetrating borehole into gas reservoirs. *Transport In Porous Media* 91:889–911.

Nooner, SL, Eiken, O, Hermanrud, C, Sasagawa, GS, Stenvold, T, Zumberge, MA (2007). Constraints on the in situ density of CO_2 within the Utsira formation from time-lapse seafloor gravity measurements. *International Journal of Greenhouse Gas Control* 1:198-214

Nordbotten, JM, Celia, MA and Bachu, S (2005). Injection and storage of CO_2 in deep saline aquifers: analytical solution for CO_2 plume evolution during injection. *Transport In Porous Media*, 58:339–360.

Nordbotten, JM and Celia, MA (2006). Similarity solutions for fluid injection into confined aquifers. *Journal of Fluid Mechanics*, 561:307-327.

Olivella, S, Carrera, J, Gens, A and Alonso, EE (1994). Non-isothermal multiphase flow of brine and gas through saline media. *Transport In Porous Media*, 15:271–93.

Olivella, S, Gens, A, Carrera, J and Alonso, EE (1996). Numerical formulation for a simulator (CODE_BRIGHT) for the coupled analysis of saline media. *Eng. Computations*, 13:87–112.

Pau, GSH, Bell, JB, Pruess, K, Almgren, AS, Lijewski, MJ and Zhang, K (2010). High resolution simulation and characterization of density-driven flow in CO_2 storage in saline aquifers, *Advances in Water Resources*, 33(4):443-455.

Riaz, A, Hesse, MA, Tchelepi, HA and Orr, FM Jr (2006). Onset of convection in a gravitationally unstable boundary layer in porous media. *Journal of Fluid Mechanics*, 548:87-111.

Rutqvist, J, Birkholzer, JT, Cappa, F and Tsang, C-F (2007). Estimating maximum sustainable injection pressure during geological sequestration of CO_2 using coupled

fluid flow and geomechanical fault-slip analysis. *Energy Conversion & Management*, 48:1798–1807.

Saripalli, P and McGrail, P (2002). Semi-analytical approaches to modeling deep well injection of CO_2 for geological sequestration. *Energy Conversion & Management* 43:185-198.

Span, R and Wagner, W (1996). A new equation of state for carbon dioxide covering the fluid region from the triple-point to 1100 K at pressures up to 88 MPa. *Journal Phys Chem Ref Data*, 25 (6):1509-1596.

van Genutchen, R (1980). A closed-form equation for predicting the hydraulic conductivity of unsaturated soils. *Soil Sci. Soc. Am. J.*, 44:892-898.

Vilarrasa, V, Bolster, D, Dentz, M, Olivella, S and Carrera, J (2010a). Effects of CO_2 compressibility on CO_2 storage in deep saline aquifers. *Transport In Porous Media*, 85(2):619-639.

Vilarrasa, V, Bolster, D, Olivella, S and Carrera, J (2010b). Coupled hydromechanical modeling of CO_2 sequestration in deep saline aquifers. *International Journal of Greenhouse Gas Control*, 4(6):910-919.

Vilarrasa, V, Silva, O, Carrera, J and Olivella, S (2012). Liquid CO_2 injection for geological storage in deep saline aquifers. *International Journal of Greenhouse Gas Control*, *submitted*.

Zhou, Q, Birkholzer, J, Tsang, C-F and Rutqvist, J (2008). A method for quick assessment of CO_2 storage capacity in closed and semi-closed saline formations. *International Journal of Greenhouse Gas Control*, 2:626–39.

FIGURES

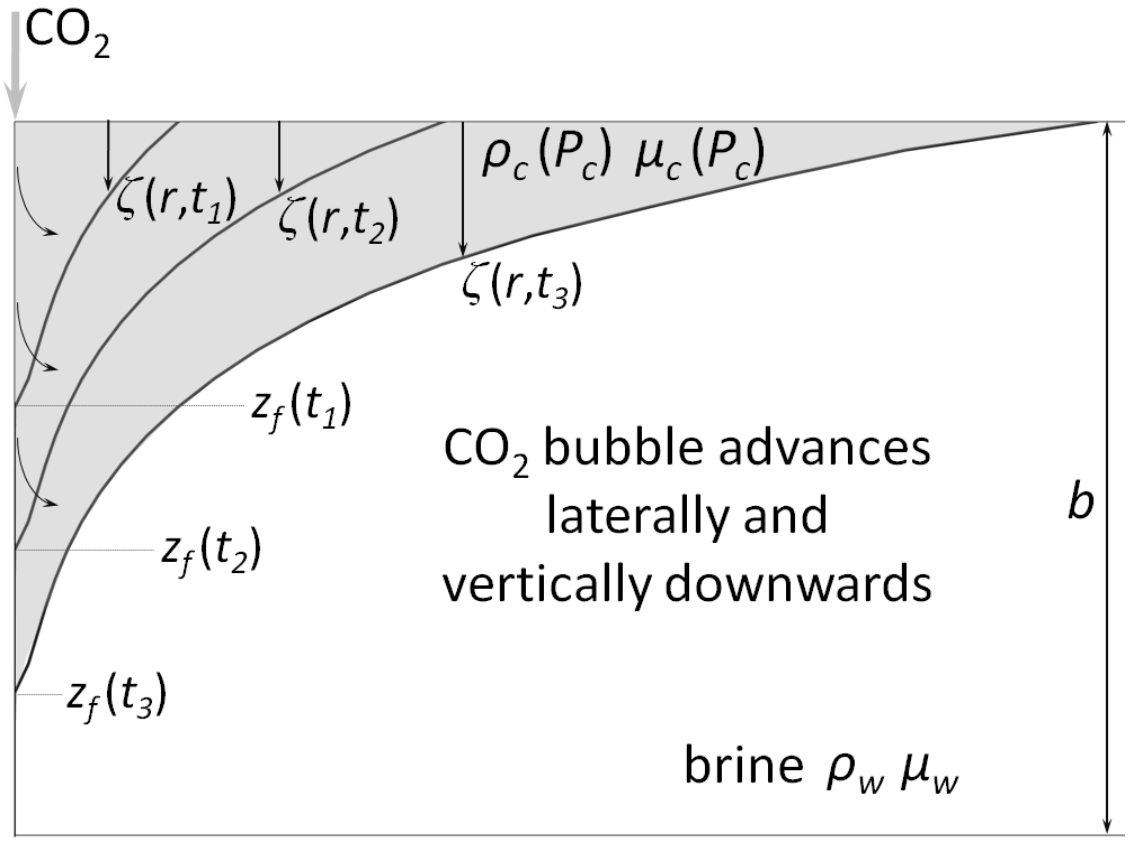

Figure 1. CO_2 injection in a deep saline aquifer. The CO_2 plume thickness at the injection well progressively increases with time as CO_2 pressure builds up. CO_2 density and viscosity are dependent on pressure. Note that CO_2 remains in the upper part of the aquifer because of buoyancy and it is not necessarily injected through the whole thickness of the aquifer.

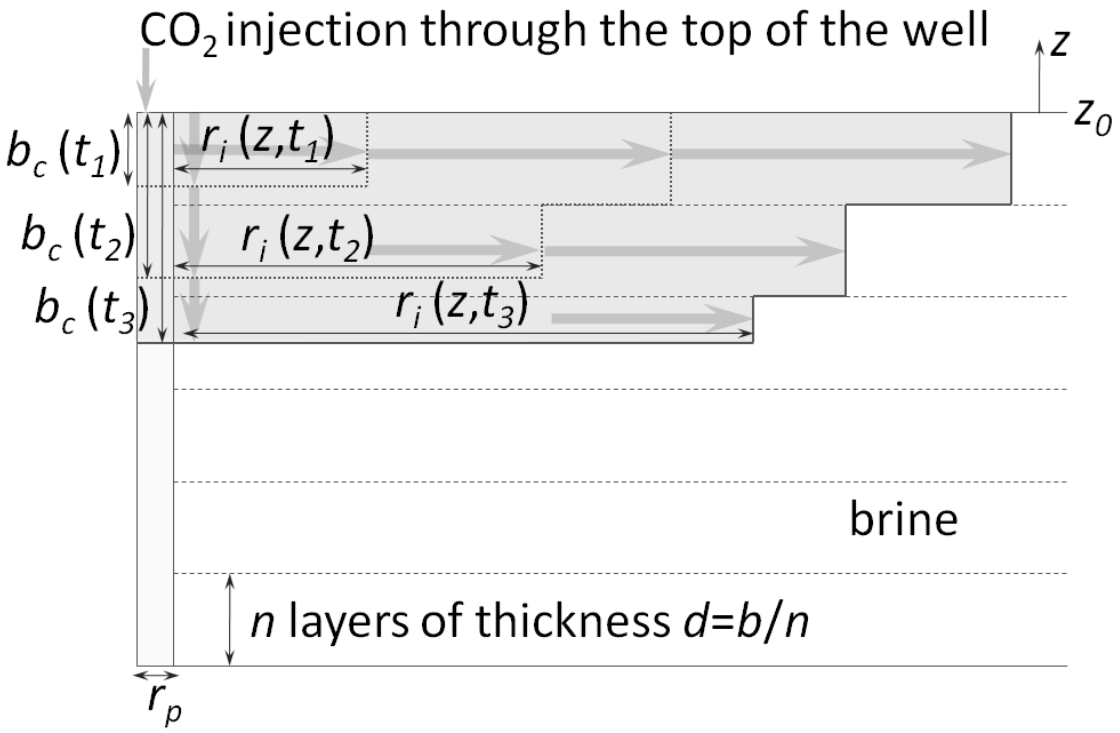

Figure 2. Schematic representation of CO_2 injection evolution taking into account that CO_2 first enters through the top of the aquifer because of buoyancy. The aquifer is divided into *n* layers through which CO_2 advances laterally and vertically downwards. The CO_2 plume at the well reaches, at every time step, the depth at which CO_2 pressure equals brine pressure.

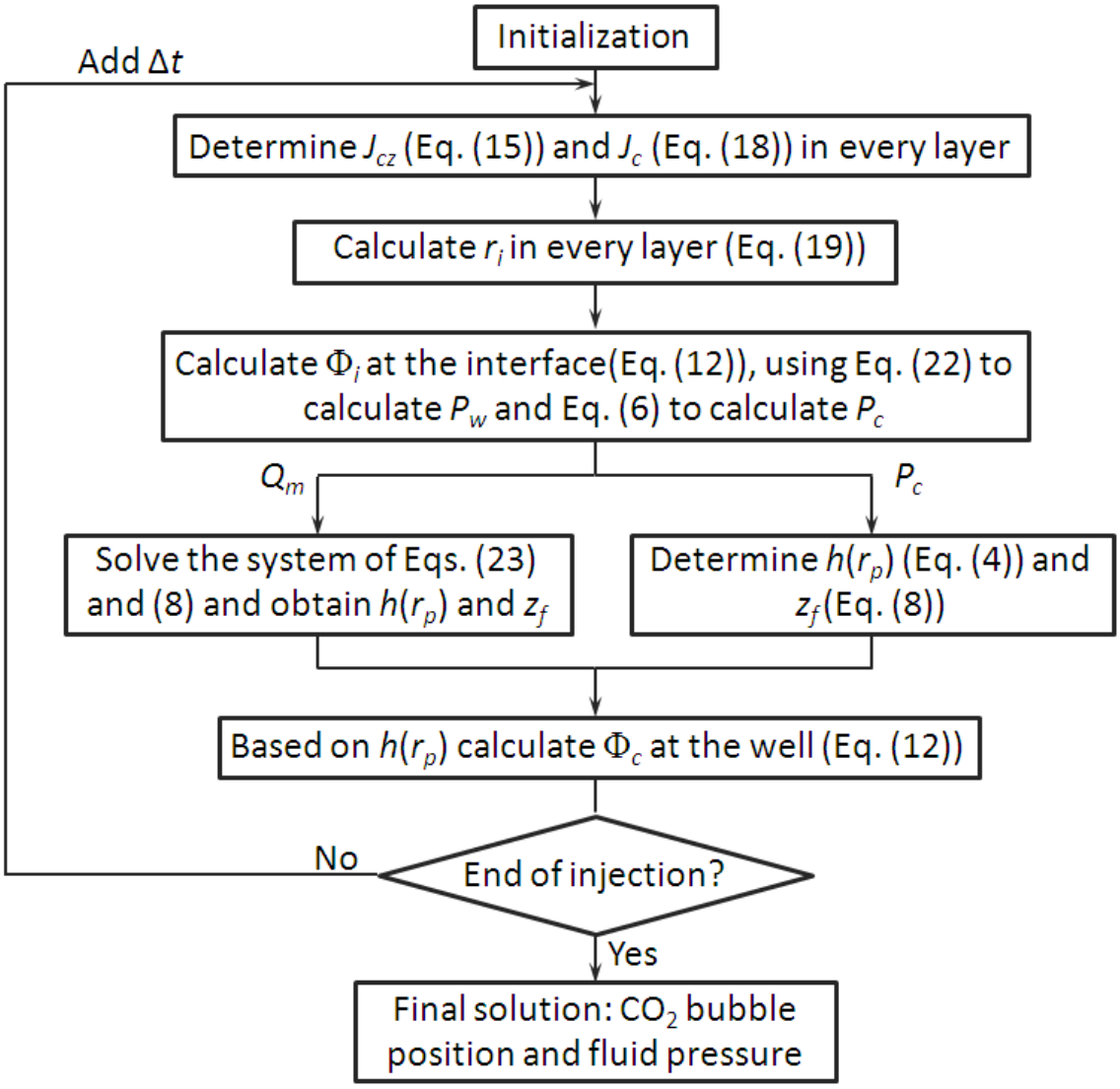

Figure 3. Time stepping algorithm to calculate the position of the CO_2 plume and the fluid pressure.

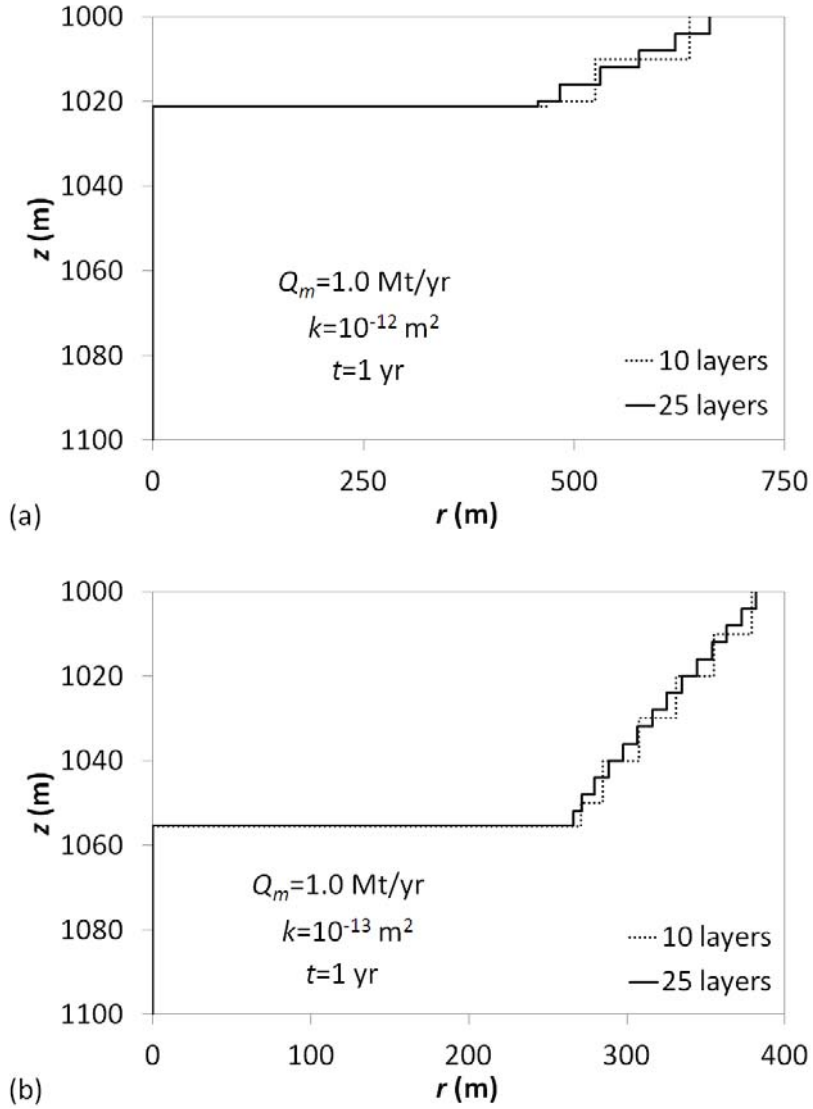

Figure 4. Effect of the number of layers (10 or 25 layers) contained in the semianalytical solution, without incorporating vertical flows, on the CO_2 plume position, after 1 yr of injection of 1 Mt/yr, for permeabilities, k, (a) $k = 10^{-12}$ m^2 and (b) $k = 10^{-13}$ m^2. Note that the differences are small and that become negligible as the number of layers increases further.

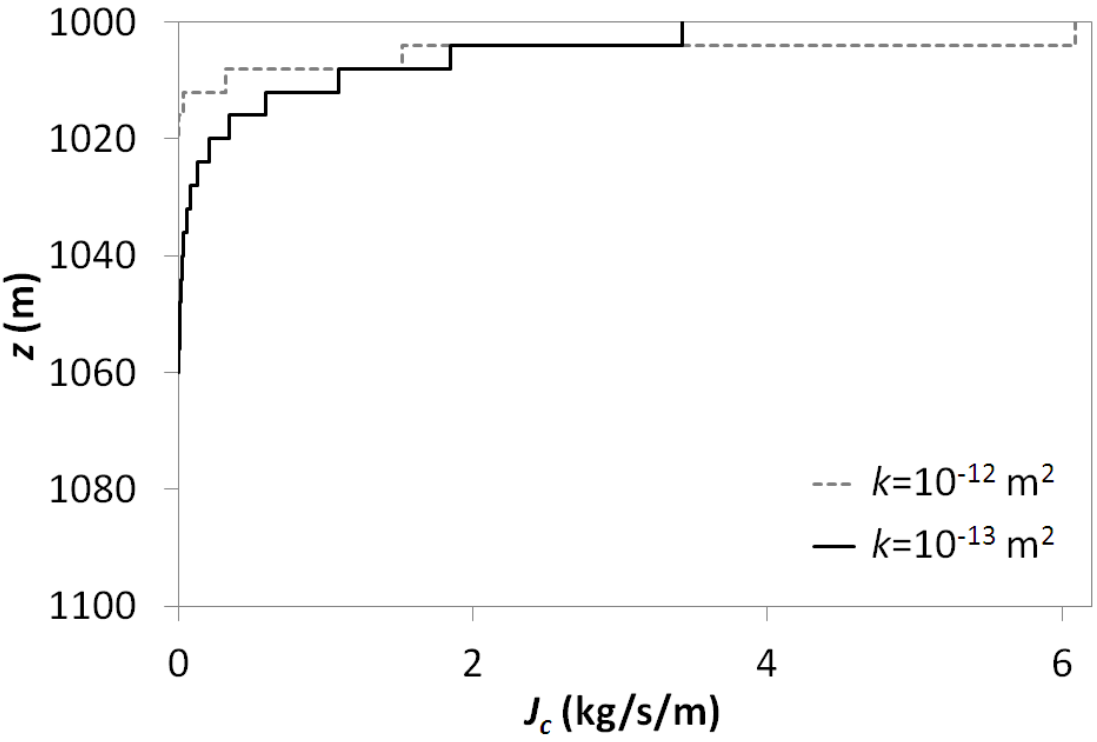

Figure 5. CO_2 mass flow rate per unit thickness at the injection well as a function of depth after 1 year of injecting 1 Mt/yr for two permeabilities. Note that in both cases the vast majority of CO_2 is injected through the top portion of the aquifer, rather than being uniformly injected along the whole thickness of the aquifer.

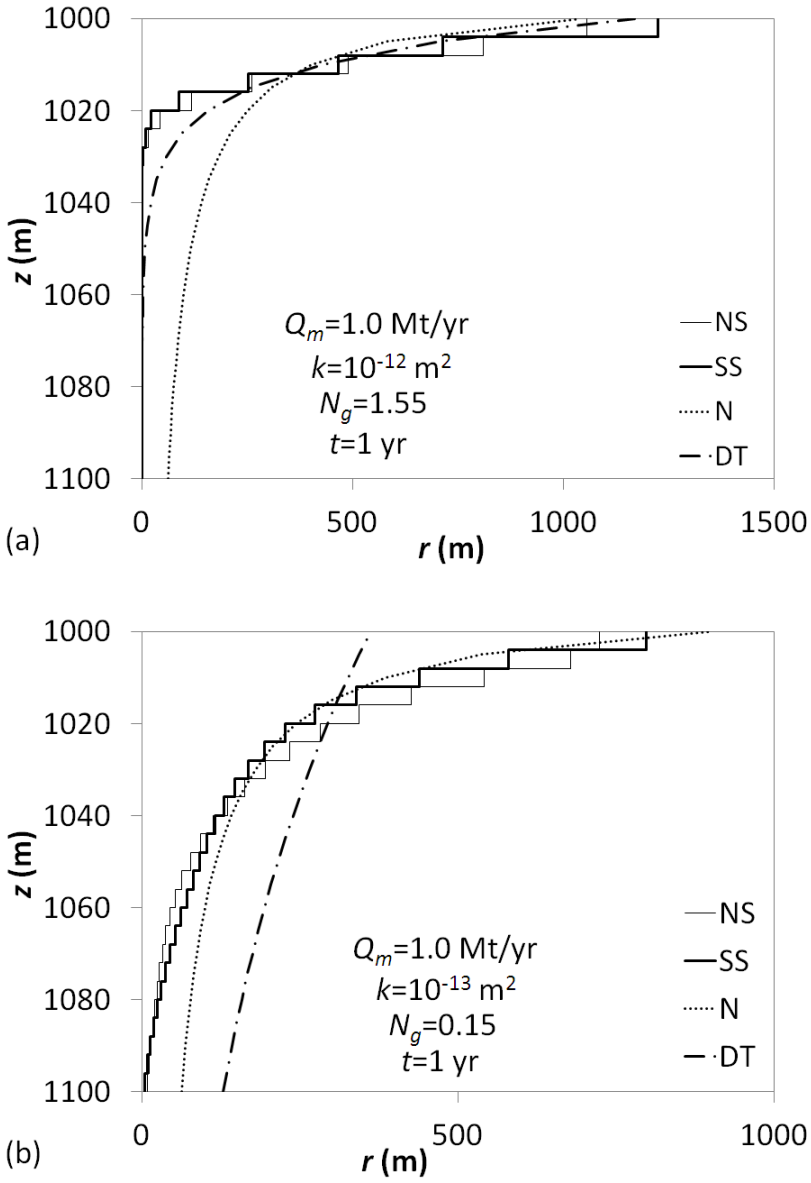

Figure 6. Comparison of the CO_2 plume position between semianalytical (SS) and numerical solution (NS) after 1 yr of injection of 1 Mt/yr, and permeabilities, k, (a) k = 10^{-12} m^2 and (b) k = 10^{-13} m^2. Additionally, the analytical solutions of Nordbotten *et al.* (2005) (N) and Dentz and Tartakovsky (2009a) (DT) after using the method of Vilarrasa *et al*. (2010a) to account for CO_2 compressibility are presented for comparison. Note that these analytical solutions inject CO_2 uniformly along the whole thickness of the aquifer.

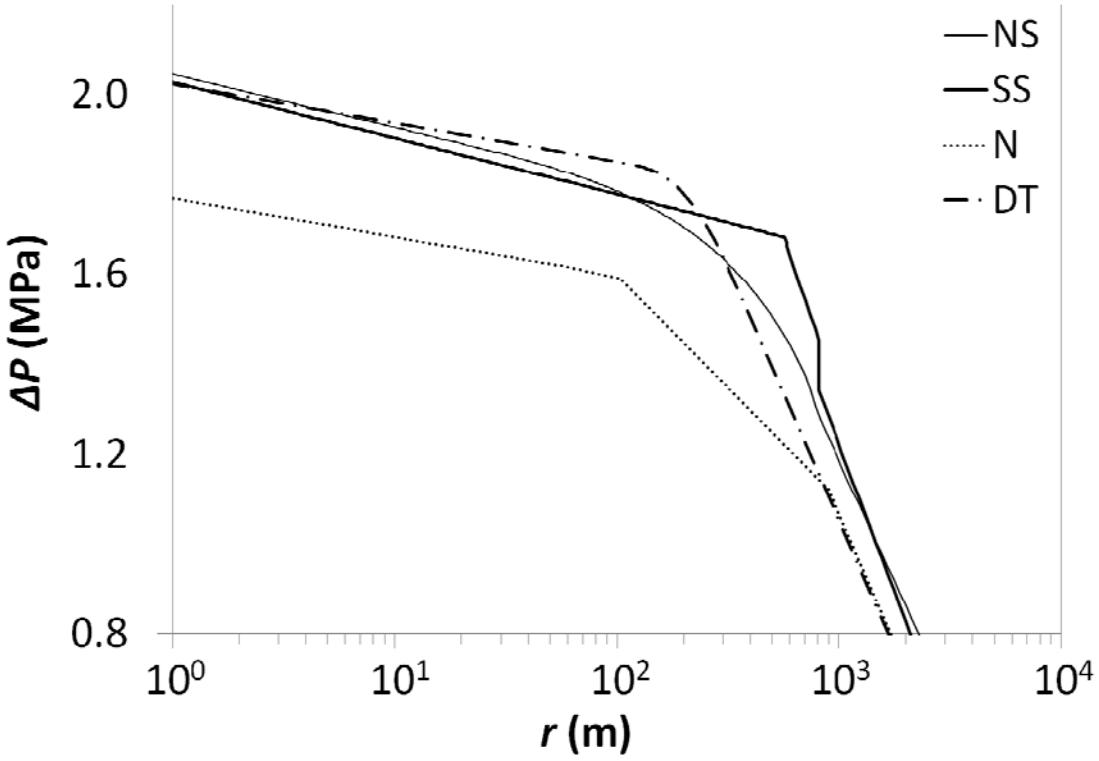

Figure 7. Comparison of the fluid overpressure at the top of the aquifer between analytical, semianalytical (SS) and numerical solutions (NS) after 1 yr injecting 1.0 Mt/yr in an aquifer with a permeability of 10^{-13} m^2. The analytical solutions of Nordbotten *et al.* (2005) (N) and Dentz and Tartakovsky (2009a) (DT) after using the method of Vilarrasa *et al*. (2010a) to account for CO_2 compressibility are presented for comparison. The first change in slope beginning from the right hand side of the figure indicates the CO_2-brine interface position for each solution.

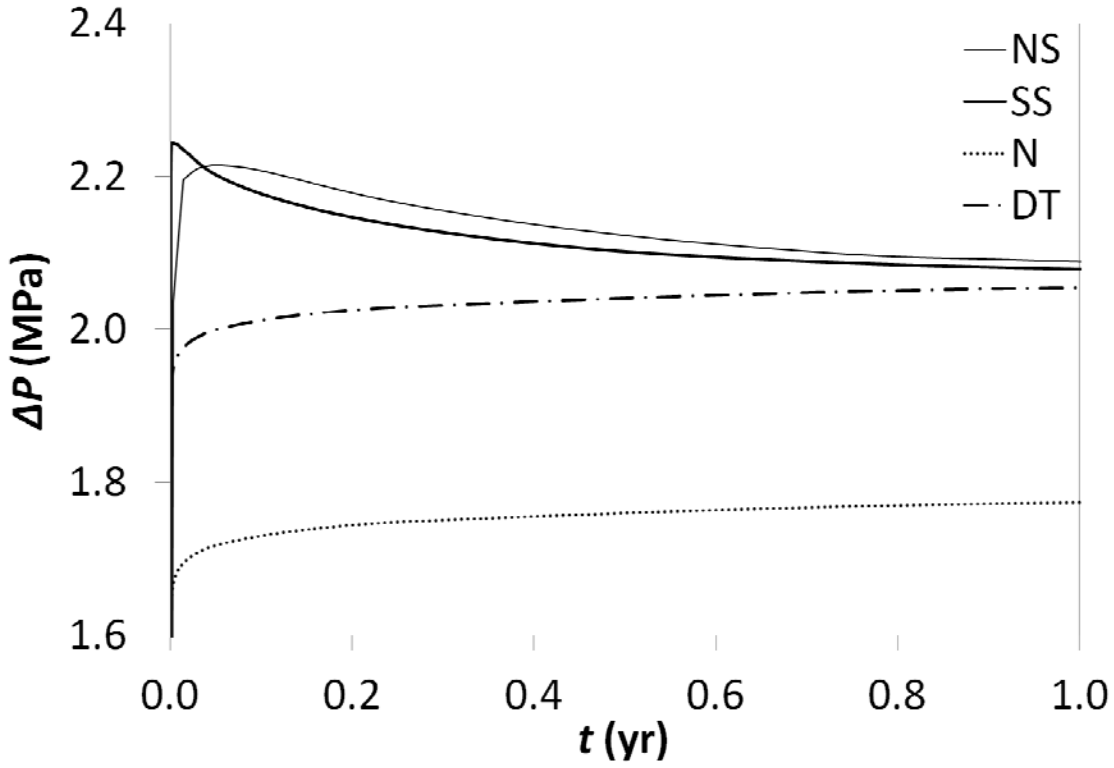

Figure 8. Comparison of the time evolution of the injection pressure at the top of the aquifer between analytical, semianalytical (SS) and numerical solutions (NS) when injecting 1.0 Mt/yr in an aquifer with a permeability of 10^{-13} m^2. The analytical solutions of Nordbotten *et al*. (2005) (N) and Dentz and Tartakovsky (2009a) (DT) after using the method of Vilarrasa *et al*. (2010a) to account for CO_2 compressibility are presented for comparison.

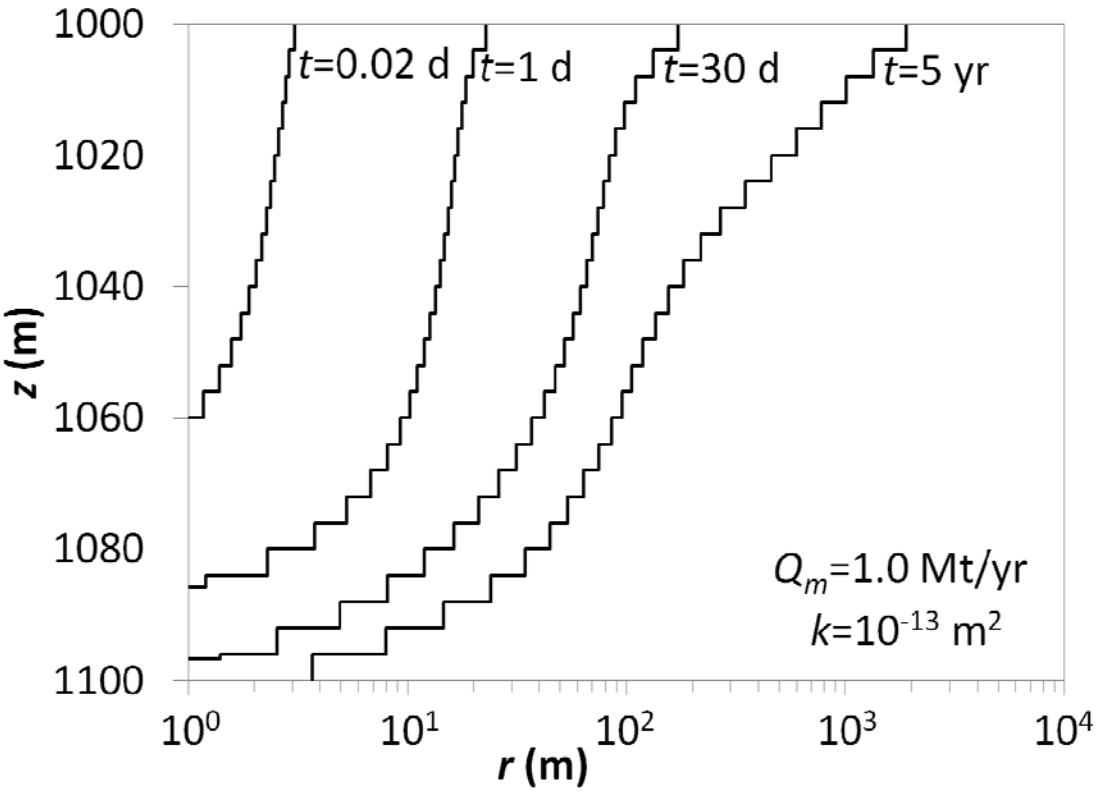

Figure 9. CO_2 plume evolution given by the semianalytical solution for several injection times when injecting 1.0 Mt/yr in a 100 m thick aquifer with a permeability of 10^{-13} m^2. Note that the thickness of the CO_2 plume progressively increases with injection time.

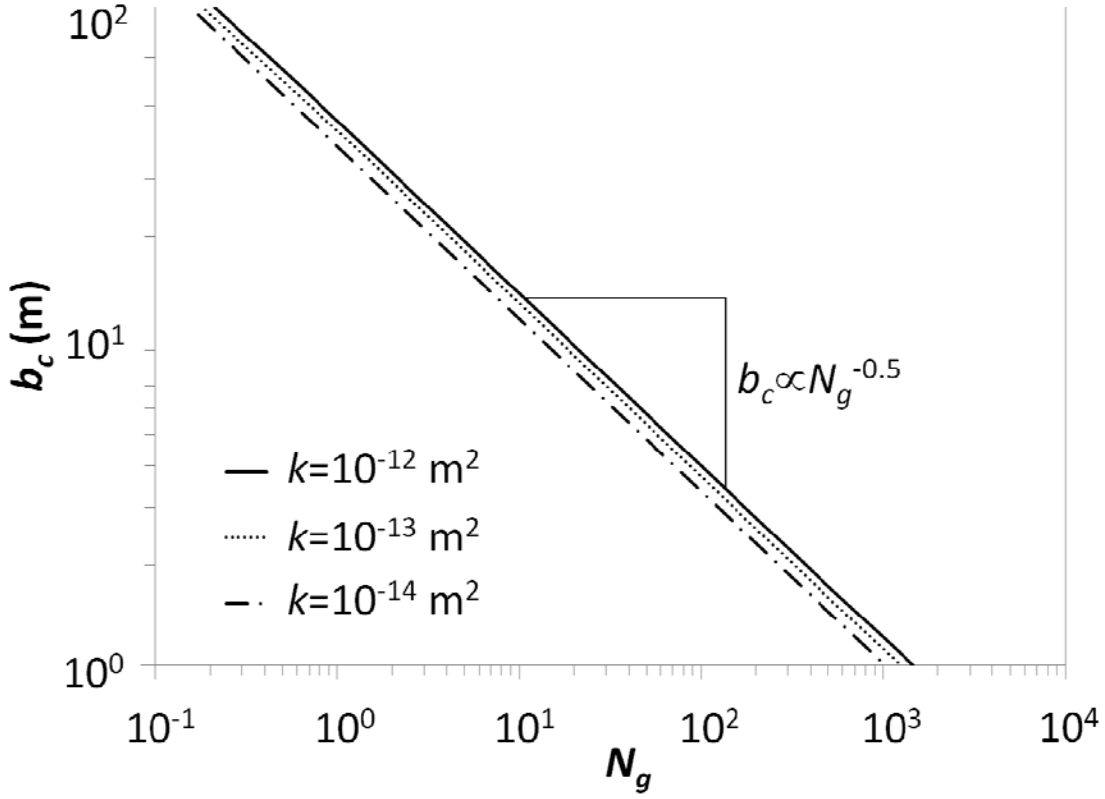

Figure 10. CO_2 plume thickness at the injection well after 1 yr of injection as a function of the gravity number for several aquifer permeabilities. Note that the logarithm of the CO_2 plume thickness decreases linearly with the logarithm of the gravity number.